

Rotational Capacity of Beam-Column with High Strength Steel

H. S. Joo, J. Moon, J. K. Kim, and H. E. Lee

Abstract—Application of high strength steel to stiffened girder of cable stayed bridge has the advantage of saving steel. However, it is generally known that the rotational capacity (ductility) of the high strength steel is smaller than that of conventional steel, and application of high strength steel can cause ductility problems in bridge. The rotational capacity of Beam-column is a crucial design parameter in stiffened girder of cable stayed bridge. In this study, high strength steel with yield stress of 690MPa was used. The rotational capacity of the beam-column with high strength steel was derived based on the stress-strain curve of high strength steel. The theoretical model was verified through a series of experimental results and parametric study.

Index Terms—Ductility, rotational capacity, high strength steel, beam-column cable-stayed bridges.

I. INTRODUCTION

The stiffened girder of cable-stayed bridges may be regarded as beam-column [1]. Beam-column is the structure subjected the axial compressive force and the flexural bending moment. It is well known that a large bending moment and axial compressive force occur in stiffened girder near the tower. In initial stage of cable-stayed bridges, only axial compressive force is applied due to adjust cable initial tension. When live load is applied, axial compressive force and the flexural bending moment are increased with the ratio of compressive force and bending moment a (see Fig. 1). The application of high strength steel can cause ductility problems for composite section [2]. Nakashima [3] suggested a trend of rotational capacity of beam-columns by the slenderness ratio. Chrysanthopoulos *et al.*, [4] proposed theoretical equation of rotational capacity of beam-columns and suggested trend of rotational capacity by the probabilistic method. These researches are considered material property based on normal strength steel. Thus, this paper suggested predicted method of rotational capacity of non-composite and composite beam-column with high strength steel and verified through the experimental study and parametric study.

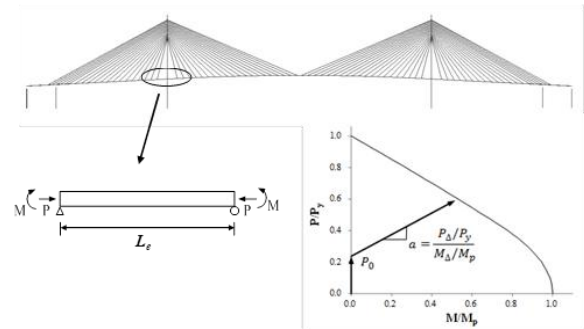


Fig. 1. Stiffened girder and analytical model.

II. ROTATIONAL CAPACITY OF BEAM-COLUMN

A. Characteristics of High Strength Steel

Research of plastic behavior of beam-column structures should be carefully examined for application to beam-column with high strength steel since the rotational capacity mainly results from the material properties of the steel, and the yield stress of the steel has recently become increased. Fig. 2 shows the stress-strain curve for high strength steel and normal strength steel from the results of coupon test. The characteristics of a stress-strain curve for high strength steel that distinguishes it from that for normal strength steel is that the plastic plateau is negligibly small, as shown in Fig. 1 Thus, strain hardening appears immediately after yielding, and yield strain and strain at the initiated point at which strain hardening are almost the same. These characteristics cause the ductility problems of the beam-column with high strength steel.

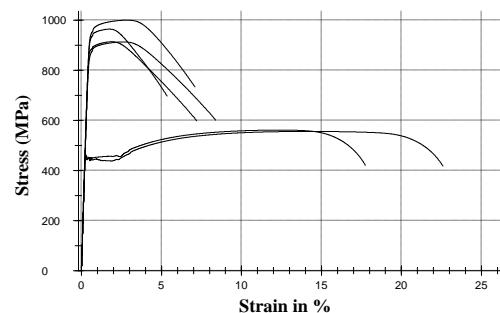


Fig. 2. Stress-strain curve of normal strength steel and high strength steel.

B. Effective Plastic Moment of Beam-Column

Fig. 3 shows the analytical model of simply supported beam-column subjected axial compressive force and bending moment. Maximum moment occur at mid span by axial compressive force and bending moment. When increasing the axial compressive force and bending moment, the cross

Manuscript received November 20, 2013; revised January 8, 2014. This work was supported in part by the Ministry of Land, Transport and Maritime Affairs (MLTM) through the Super Long Span Bridge R&D Center in Korea.

The authors are with the School of Civil, Environmental and Architectural Engineering, Korea University, Seoul 136-713, South Korea (e-mail: obladaia@korea.ac.kr, jmoon1979@korea.ac.k, player90@nate.com, helee@korea.ac.kr).

section reaches the plastic stage. Fig. 4 shows that the stress diagram changes as the applied moment is increased for an applied axial force. The fundamental concepts are that strains linearly distributed across the cross section are related to stresses using an elasto-plastic model. Compressive flange reaches to yield stress first.

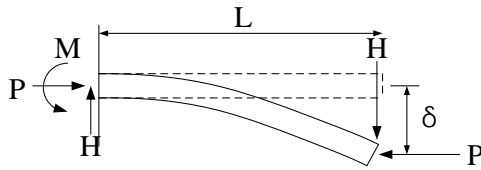


Fig. 3. Analytical model

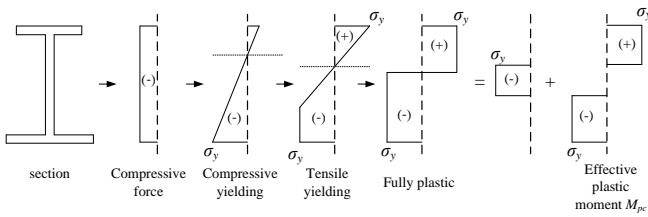


Fig. 4. Stress distribution under axial force and bending moment.

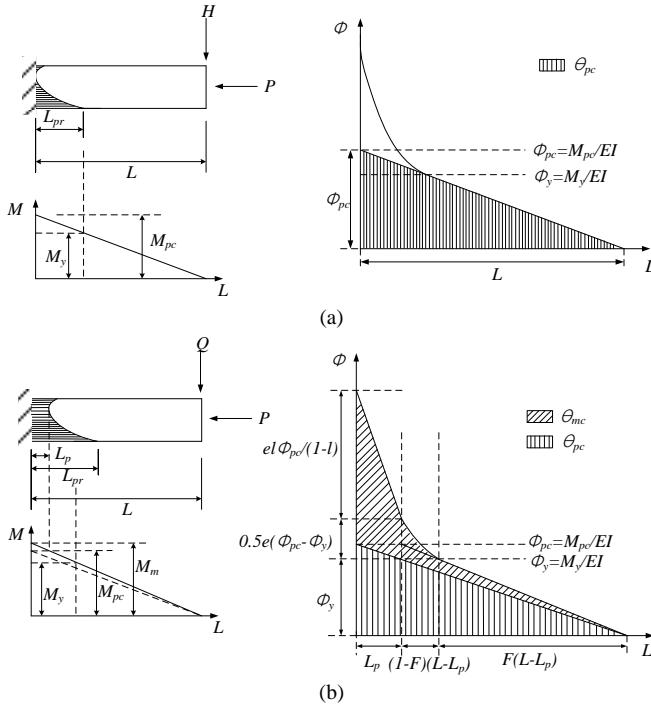


Fig. 5. Theoretical model: (a) at M_{pc} ; (b) at M_{mc} .

The presence of axial compression force reduces the full plastic moment capacity of a section of beam-column. This reduced plastic moment capacity of a section considering the influence of axial compressive force is designated the effective plastic moment M_{pc} . Fig. 4 shows stress diagram at plastic stage of analytical model. The axial compressive force is assumed to be entirely by a centrally located portion of the total cross sectional area stressed to the yield stress in compression.

C. Theoretical Derivation of the Available Rotational Capacity

Joo *et al.*, [5] proposed equations to estimate the available rotation capacity of the non-composite I-girder and composite

I-girder with high strength steel in negative moment region based on a material property of high strength steel, respectively. In this chapter, that approach was modified to estimate the available rotational capacity of beam-column with high strength steel.

Figs. 5. (a) and (b) show the yielding region, bending moment, and curvature diagrams at the effective plastic moment M_{pc} and effective maximum bending moment M_{mc} , respectively. L_{pr} denotes the yield length, where it is defined as the distance from the loading point to the extreme fiber that is yielded. L_p is the plastic length, where L_p can be obtained from the distance from the loading point to the point of the cross-section that is fully yielded. θ_{pc} is the rotation corresponding to elastic limit. θ_{mc} is the rotation corresponding to M_{mc} . Based on the stress-strain curve shown in Fig. 2, the curvature distribution can be obtained as Fig. 5. (b). Then, the shade area in Fig. 5. (b) represents the plastic rotation corresponding to the maximum effective moment resistance of the section, M_{mc} . The plastic length L_p must be determined first. Kemp & Dekker [6] proposed L_p considering the inelastic lateral-torsional buckling and local buckling of the flange and the web. In this study, L_p proposed by Kemp & Dekker [6] was used.

III. EXPERIMENTAL STUDY

An experimental study was conducted to verify the suggested method for rotational capacity of beam-column with high strength steel. Six non-composite singly symmetric I-sections were fabricated. The tested specimens denoted throughout this paper as M1-1 to M1-3 and M2-1 to M2-3. Specimens M1-1 to M1-3 and M2-1 to M2-3 were fabricated same dimensions and material, respectively. The length of all specimens L is 2,600mm and thickness of flange and web is 15mm. In specimens M1, the width of the bottom flange b_{fc} was 100 mm, the width of the top flange b_{ft} was 70 mm, and depth of web d_w is 185mm. In specimens M2, the width of the bottom flange b_{fc} was 100 mm, the width of the top flange b_{ft} was 50 mm, and depth of web d_w is 150mm. The specimens were fabricated from high strength steel, and the stress-strain curve was obtained from the material test. The detailed dimensions of test specimens and results of specimens are shown in Table I. Where t_{fc} is the bottom flange thickness; t_{ft} is the top flange thickness; and t_w is the web thickness, respectively.

TABLE I: DIMENSIONS AND RESULTS OF SPECIMENS

Model	Dimensions (mm)	Initial Compressive Load P (kN)	Ultimate flexural load Q (kN)
M1-1	$L: 2,600; b_{fc}: 100$	0	280
M1-2	$b_{ft}: 70; d_w: 185$	200	265
M1-3	t_{fc}, t_{ft} and $t_w: 15$	400	225
M2-1	$L: 2,600; b_{fc}: 100$	0	199
M2-2	$b_{ft}: 50; d_w: 150$	200	176
M2-3	t_{fc}, t_{ft} and $t_w: 15$	400	155

The main parameter was the ratio of compressive force and bending moment. M1-1 and M2-1 were tested under pure bending moment. M1-2, M1-3, M2-2, and M2-3 were tested

under combined initial axial compression force and an increasing level of applied bending moment. A combination of load actuators was used to produce axial compressive loads and bending moments in the specimens. Fig. 6 shows schematic view and boundary conditions of test specimens. The vertical load was applied using 1,000 kN-capacity actuator placed in the frame for the axial compressive load. The horizontal load was applied using 1,000 kN-capacity actuator with usable stroke of 300mm placed in the rigid support for the bending moment. The resulting moment in each tested specimen was calculated taking into account the equilibrium of the external forces acting on it. The following equation was used to calculate the bending moment in each step:

$$M = \frac{QL + P\delta}{2} \quad (1)$$

where δ is the measured horizontal displacement at loading point (see Fig. 6). Model M1-1 and M2-1 were subjected pure bending moment. The other specimens were subjected initial compressive force P , after that were subjected load Q to induce a bending moment.

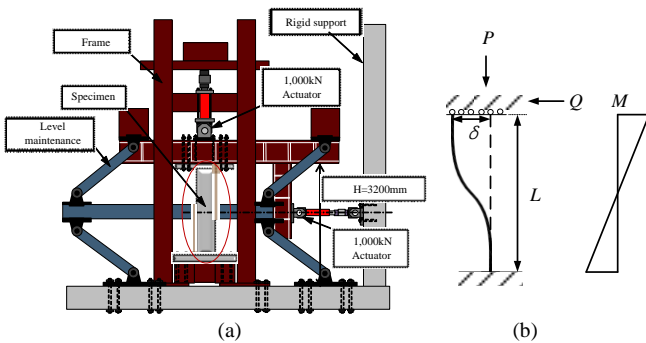


Fig. 6. Schematic view: (a) Test set up; and (b) Boundary condition and moment diagram

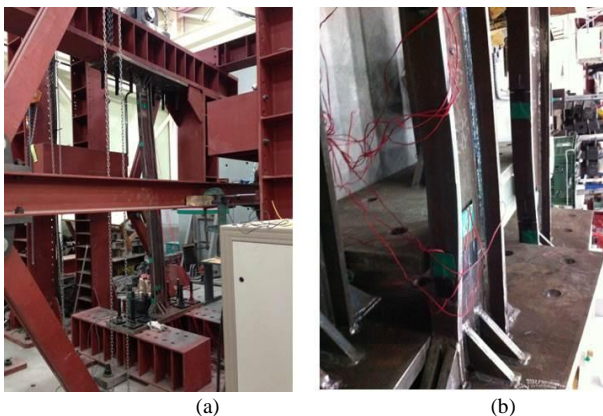


Fig. 7. Test view: (a) test set up; and (b) deformed shape of specimen

Fig. 7 shows the deformed shape of test specimen after the test was completed. From the results of load and displacement data, it is possible to determine the normalized moment-deflection curves for the test specimens M1 and M2 are shown in Fig. 7. The x and y axes in Fig. 8. (a) represent the deflection at loading point δ normalized by half length of the specimen $L/2$, and the applied moment M normalized by the plastic moment when specimen subjected pure bending moment M_p , respectively. M1 series and M2 series had the

almost effective plastic moment M_{pc} , respectively. However, maximum moment of test results has the difference due to the influence of the axial compressive load. Fig. 8. (a) shows that maximum moment larger than predicted plastic moment.

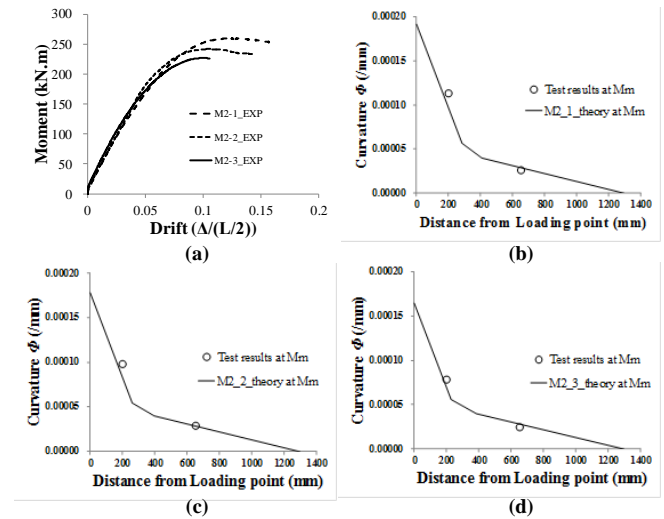


Fig. 8. Test results: (a) Normalized moment-deflection curve; (b) Curvature distribution of M2-1; (c) Curvature distribution of M2-2; and (d) Curvature distribution of M2-3

The curvature of the test specimens was calculated from the strain data, and compared with the theoretical curvature distribution derived in this study (see Fig. 5). Fig. 8. (a) to (c) compares the curvature distribution proposed in this study with the test results. It can be seen that the theoretical curvature distribution proposed in this study agrees well with the test results for specimens as shown in Fig. 8. (a) to (c).

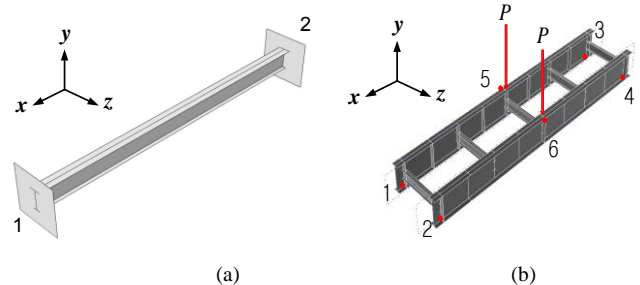


Fig. 9. Loading and boundary condition of the analysis model: (a) model for test setup; and (b) simple model

IV. PARAMETRIC STUDY

A series of parametric studies were performed for further verification of available rotational capacity of high strength steel beam-column. To verify the experimental study, a nonlinear three-dimensional finite element analysis models were constructed to simulate the test specimens. The structural analysis program ABAQUS [7] was used. A 4-node shell element with reduced integration (S4R) was used to construct the flange and web of the analysis models. Fig. 9. (a) shows the loading and the boundary conditions of the test set-up. To simulate one end fixed and the other end guided beam-column, stiffeners were constructed at both ends for preventing rotation. And, the x , y and z directions at point 1 and the x and z directions at point 2 were restrained. And, axial compressive load was applied in x direction at both ends, and load was applied in y direction to induce a bending

moment at point 2. In order to generalize the results and to consider a broader range of sections, different boundary conditions and effects of cross beam, additional finite element analysis was conducted. Fig. 9. (b) shows the loading and the boundary conditions to simulate the simply supported beam and cross beam. The y direction at point 1 and 3, and the y and z directions at point 2, 4, 5 and 6 were restrained. Finally, axial compressive load was applied in x direction at point 1, 2, 3 and 4, and load was applied in y direction to induce a bending moment at point 5 and 6.

Fig. 10. (a) and (b) show comparisons of the analysis results with the test results for M1 series and M2 series models, respectively. The analysis results agree well with the test results, and finite element analysis was successfully verified.

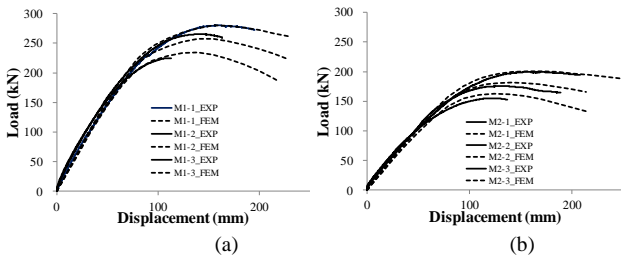


Fig. 10. Comparison of analysis results with test results: (a) M1; and (b) M2

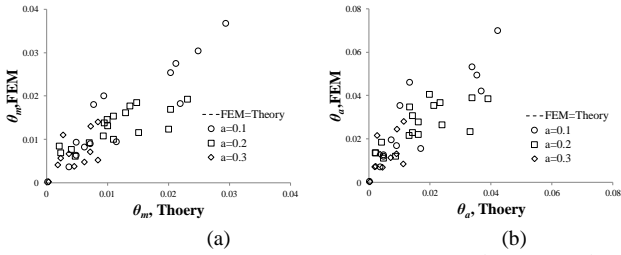


Fig. 11. Comparison of FEM results and theory: (a) θ_{mc} ; and (b) θ_a

A parametric study was conducted to verify the proposed equations of for a broader range of sections and the ratio of bending moment and axial compressive force. A total of 45 models were analysed, and the details of the analysis models are shown in Table II. The main parameters were compressive flange slenderness ratio λ_{fc} where $\lambda_{fc}=b_{fc}/(2t_{fc})$, web slenderness ratio λ_w where $\lambda_w=2D_{cp}/t_w$, unbraced slenderness ratio λ_L where $\lambda_L=L_b/\gamma_r$, and the ratio of bending moment and axial compressive force a where $a=\Delta P/\Delta M$, respectively. Three different a values ($a=0.1, 0.2, \text{ and } 0.3$) were selected to investigate the effect of the ratio of bending moment and axial compressive force on rotational capacity. The detail of range of the parameter is shown in Table II.

TABLE II: ANALYSIS MODELS FOR PARAMETRIC STUDY

Parame ters	λ_f/λ_{pf}	λ_w/λ_{pw}	λ_L/λ_{pL}	Material Model	a
Range	0.33- 0.94	0.44-0. 91	0.69-3. 01	Case1:	
				$f_y=690\text{MPa},$	Case1: 0.1
				$f_u=800\text{MPa}$	Case2: 0.2
				Case2:	
				$f_y=745.4\text{MPa},$	Case3: 0.3
				$f_u=874.2\text{MPa}$	

Fig. 11. shows a comparison of the results of θ_{mc} obtained from Fig. 5. with those obtained from finite element analysis. The x axis represents θ_{mc} obtained from Fig. 5 and the y axis denotes θ_{mc} obtained from finite element analysis, and θ_{mc} was directly calculated from the moment-rotation curve obtained from finite element analysis. From the comparative results, it can be seen that Fig. 5. provides reasonable estimation of θ_{mc} and θ_a .

V. ROTATIONAL CAPACITY OF COMPOSITE BEAM-COLUMN

A. Theoretical Derivation of the Available Rotational Capacity

In order to obtain the available rotational capacity of composite beam-column, the elastic limit rotation θ_{pc} should be calculated firstly. The elastic limit rotation θ_{pc} of flexural beam and non-composite beam column is calculated simply using flexural stiffness EI . However, flexural stiffness EI of composite beam-column in negative moment region depends on the elastic neutral axis. Fig. 11. shows that the contribution of the strain distribution according to the initial axial compressive force, additional axial compressive force, and additional bending moment. Thus, total strain distribution is sum of each contribution. Equations of strain distribution of each contribution are defined as:

$$\epsilon_{P0} = \frac{P_0}{E_s(A_c/n + A_s + A_r)} \tag{2}$$

$$\epsilon_{P\Delta} = \frac{P_\Delta}{E_s(A_c/n + A_s + A_r)} \tag{3}$$

$$\epsilon_{M\Delta} = \frac{M_\Delta y_m}{EI_{eff}} \tag{4}$$

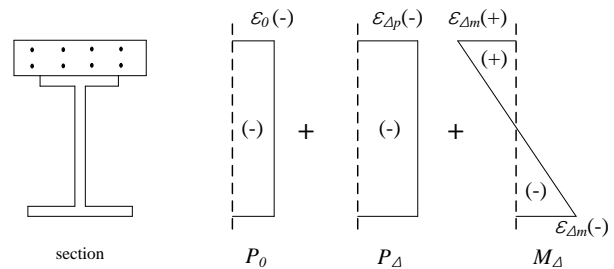


Fig. 11. Contribution of strain distribution according to the axial compressive force and bending moment

In eq. (2). to (4)., P_0 and ϵ_{P0} are the initial axial compressive force and its strain, respectively. P_Δ and $\epsilon_{P\Delta}$ are the additional axial compressive force and its strain, respectively. M_Δ and $\epsilon_{M\Delta}$ are the bending moment and its strain, respectively. Where n (the ratio of concrete elastic modulus and steel elastic modulus) is defined as E_s/E_c , y_m is the distance from elastic neutral axis of pure bending in section (see Fig. 11.), and EI_{eff} is the effective flexural stiffness of composite beam-column. Effective flexural stiffness of composite beam-column EI_{eff} is depends on the elastic neutral axis of composite section due to increase the axial compressive force

and the bending moment. Fig. 12 shows the position of elastic neutral axis due to increase the axial compressive force and the bending moment.

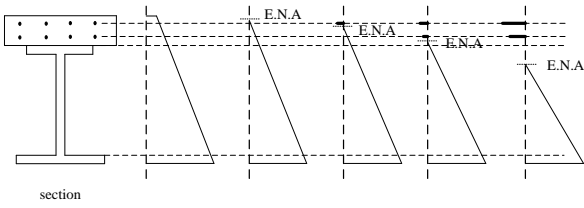


Fig. 12. Location of elastic neutral axis due to increase the axial compressive force and the bending moment

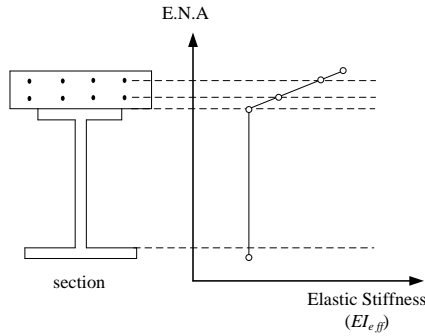


Fig. 13. Effective flexural stiffness due to location of elastic neutral axis

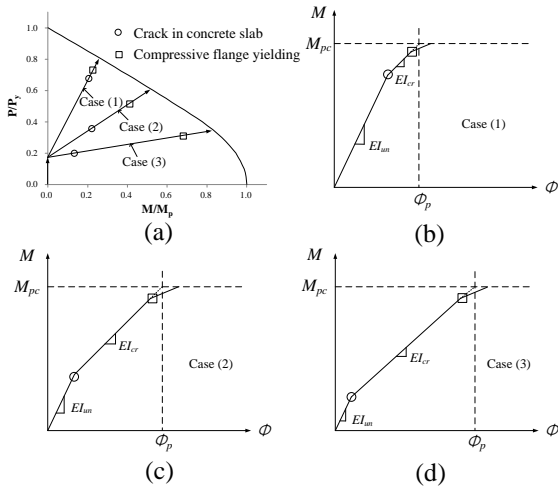


Fig. 14. Elastic behavior of stiffened girder in negative moment region according to ratio a

After the initial axial compressive force, until elastic neutral axis reaches at the top of the concrete slab, cracks in the concrete slab are not occurred (location (1) in Fig. 12). In location (1), effective flexural stiffness has the same value of that of positive moment region. When the additional axial compressive force and bending moment is increased, cracks in the concrete slab are occurred (location (2) to (4) in Fig. 12). Effective flexural stiffness in location (2) to (4) is reduced linearly depending on the location of the elastic neutral axis. When the elastic neutral axis is located in the steel section, only the steel section and reinforcement steel contribute to effective flexural stiffness. The magnitude of the effective flexural stiffness due to location of elastic neutral axis is shown in Fig. 13.

Fig. 14. shows that elastic behavior of stiffened girder in negative moment region up to Φ_p according to the ratio of axial compressive force and bending moment a . In Fig. 14,

the effective flexural stiffness of composite beam-column EI_{eff} is equal to un-cracked flexural stiffness EI_{un} up to crack in concrete slab. After concrete slab is cracked, effective flexural stiffness of composite beam-column EI_{eff} is equal to un-cracked flexural stiffness EI_{cr} . It is found that the elastic behavior of stiffened girder in negative moment region depends on the ratio of axial compressive force and bending moment a .

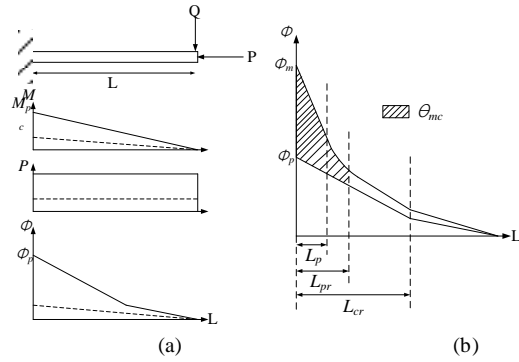


Fig. 15. Bending moment, axial force, curvature diagram of analytical model: (a) at $M=M_{pc}$; and (b) at $M=M_{mc}$



Fig. 16. Finite element analysis model

Fig. 15 (a) shows that bending moment, axial compressive force, and curvature diagram when the beam-column reaches at the effective plastic moment M_{pc} . And, dashed line represents that bending moment, axial compressive force, and curvature diagram when crack in concrete slab is not occurred. Fig. 15 (b) shows that curvature diagram when the beam-column reaches at the effective maximum plastic moment M_{mc} . L_{pr} denotes the yield length, and L_p is the plastic length. L_{cr} represents the cracked length, where L_{cr} can be obtained from the distance from the loading point to the point of the concrete slab that crack in concrete slab is not occurred. Based on the stress-strain curve, the shade area in Fig. 15 (b) represents the plastic rotation of composite beam-column with high strength steel in negative moment region.

A. Parametric Study

For the verification of the proposed available rotation capacity of the steel-concrete composite beam-column in negative moment region of the cable-stayed bridge with high strength steel, verification was conducted the based on the non-linear finite element analysis. Only negative bending moment region of stiffened girder was modeled in this chapter to evaluate the available rotation capacity. Boundary condition of the analysis model is equal to the analysis model of non-composite beam-column. Fig. 16 shows the finite element model of composite beam-column. The structural analysis program ABAQUS [7] was used for the analysis. 8-node solid element with reduced integration and 4-node shell element were used to model the concrete slab and steel

I-section, respectively. 2-node truss element was used to simulate the longitudinal and transverse reinforced rebar. Initial imperfection and residual stress of steel I-section were also considered.

The finite element analysis result was compared with proposed predicted method of rotational capacity of composite beam-column as shown in Fig. 17. The x axis of Fig. 17 represents normalized rotation angle at end of negative moment region in beam-column, and y axis represents normalized applied moment. It can be found that the proposed predicted elastic behavior up to elastic limit rotation θ_p , and the rotation represented available rotational capacity θ_m and θ_a gave the reasonable prediction of the rotational capacity of high strength steel composite beam-column.

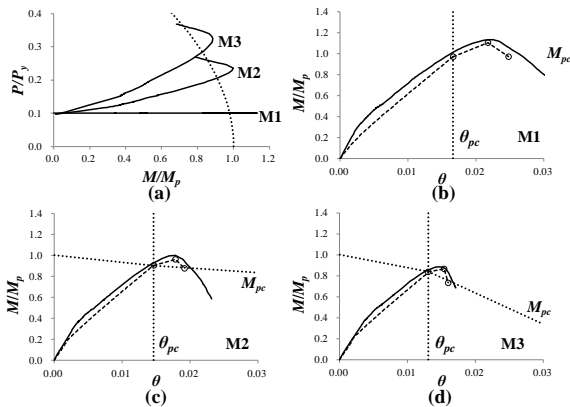


Fig. 17. Comparison of FEM results and theory: (a) normalized axial force-moment curve; (b) moment-rotation curve of M1; (c) M2; and (d) M3

VI. CONCLUSION

This paper conducted the rotational capacity of non-composite beam-column with high strength steel subjected axial compressive force and bending moment. It was proposed that the curvature distribution and method to calculate inelastic rotation of beam-column considering material characteristics of high strength steel. An experimental study was conducted to examine the validation of the proposed method. From the test results, it was found that the theoretical method in this study agrees well with the test results. This study also conducted the rotational capacity of composite beam-column with high strength considering effects of concrete slab. It was also proposed that the curvature distribution and method to calculate inelastic rotation of composite beam-column. The curvature distribution of composite beam-column should be considered elastic limit curvature using effective stiffness of composite section under magnitude of axial compressive force and bending moment. Finally, verification of proposed method was performed by using the non-linear finite element analysis. Based on the analysis results, it was found that the proposed prediction of the available rotation capacity of non-composite and composite beam-column is reasonable.

ACKNOWLEDGMENT

The authors wish to acknowledge the financial support by the Ministry of Land, Transport and Maritime Affairs

(MLTM) through the Super Long Span Bridge R&D Center in Korea.

REFERENCES

- [1] H. Yoo and D. H. Choi, "Improved system buckling analysis of effective lengths of girder and tower," *Computer and Structures*, vol. 87, pp. 847-860, 2009.
- [2] C. J. Earls and B. J. Shah, "High performance steel bridge girder compactness," *J. Construct Steel Res.*, vol. 58, pp. 859-880, 2002.
- [3] M. Nakashima, "Variation of ductility capacity of steel beam-columns," *J. Struct. Eng.*, pp. 1941-1960, 1994.
- [4] M. K. Chryssanthopoulos, G. M. E. Manzocchi, and A. S. Elnashai, "Probabilistic assessment of ductility for earthquake resistant design of steel members" *J. Construct Steel Res.*, vol. 52, 47-68, 1999.
- [5] H. S. Joo, J. Moon, B. H. Choi, and H. E. Lee, "Rotation capacity and optimum bracing point of high strength steel i-girders" *J. Construct Steel Res.*, vol. 88, 79-89, 2013.
- [6] A. R. Kemp and N. W. Dekker, "Available rotation capacity in steel and composite beams," *The Structural Engineer*, vol. 69, no. 5, pp. 88-97, 1991.
- [7] *ABAQUS Analysis User'S Manual* Version 6.9-2, Dassault Systemes Simulia Corp., Providence, RI, USA, 2009.



H. S. Joo received his M. S. from Korea University, Seoul, Korea, structural engineering in 2007. He received B. S. Korea University, Seoul, Korea, and civil engineering in 2005.

He is a Ph. D. Candidate in Korea University. Paper title of published journal is "Rotation capacity and optimum bracing point of high strength steel i-girders" in *J. Construct, Steel Res.*



M. Moon received his Ph.D form Korea University, Seoul, Korea, structural engineering (2009). He received his M. S. form Korea University, Seoul, Korea, structural engineering (2004). He received his B. S. form Korea University, Seoul, Korea, civil engineering in 2002.

He is a research professor in Korea University. Paper titles of published journal are "Analytical modeling of bending of circular concrete-filled steel tubes" in *Engineering Structures* in 2013. He paper title is "Shear strength and design of trapezoidally corrugated steel webs," in *J. Construct. Steel Res.* in 2009 and the other paper tile is "In-plane strength and design of parabolic arches" in *Engineering Structures* in 2009.

Dr. Moon is the member of Korean Society of Civil Engineers



J. K. Kim received his B.S. from Ajou University, Suwonl, Korea, and civil engineering in 2011.

He is a Ph. D. Candidate in Korea University.



H. E. Lee received his PH.D form University of Pittsburgh, Pittsburgh, USA, structural engineering in 1987. He received his M.S. from University of Pittsburgh, Pittsburgh, USA, structural engineering in 1982. He received his B.S. Korea University, Seoul, Korea, civil engineering (1980).

He is a professor in Korea University. Paper titles of published journal are "Prediction of bridge flutter under a crosswind flow" in *Wind and Structures* in 2013, "Non-linear analyses model for composite box-girders with corrugated steel webs under torsion" in *Steel and Composite structures* in 2013, and "Moment gradient correction factor and inelastic flexural-torsional buckling of I-girder with corrugated steel webs" in *Thin-Walled Structures* in 2013.

Prof. Lee is the member of Korean Society of Civil Engineers (KSCE), International Association for Bridge and Structural Engineering (IABSE), and East Asia-Pacific Conference on Structural Engineering and Construction (EASEC).